COUPLED LAGRANGIAN AND EULERIAN SIMULATION OF BUBBLY FLOWS IN VERTICAL PIPES: VALIDATION WITH EXPERIMENTAL DATA USING MULTI-SENSOR CONDUCTIVITY PROBES AND LASER DOPPLER ANEMOMETRY

José L. Muñoz-Cobo[1], Sergio Chiva[2], Santos Mendes[3], Mohamed Ali Abdelaziz[1]

1-Instituto de Ingeniería Energética, Universidad Politécnica de Valencia Spain
2- Department of Mechanical Engineering and Construction, Universitat Jaume I, Spain
3- Universidad Nacional Autónoma de Mexico (UNAM)

Abstract.

A set of two phase flow experiments for conditions ranging from bubbly flow to cap/slug flow have been performed under isothermal concurrent air-water flow conditions in a vertical column of 3 m height. Also the liquid properties like the surface tension have varied by adding small quantities of 1-Butanol in order to see how these changes affect to the two phase flow properties.
Numerical simulations of these experiments for bubbly flow conditions were performed by coupling a Lagrangian code that tracks the 3D motion of the individual bubbles in cylindrical coordinates (r,ϕ,z) inside the fluid field under the action of the following forces: buoyancy, drag, lift, wall lubrication. Also we have incorporated a 3D stochastic differential equation model to account for the random motion of the individual bubbles in the turbulent velocity field of the carrier liquid. Also we have considered the deformation that suffers the bubbles when they touch the walls of the pipe and are compressed until they rebound.
The velocity and turbulence fields of the liquid phase were computed by solving the time dependent conservation equations in its Reynols Averaged Transport Equation form (RANS). The turbulent kinetic energy k, and the dissipation rate ε transport equations were simultaneously solved by using the k, epsilon model in a (r,z) grid by the finite volume method using the SIMPLER algorithm. Both Lagrangian and Eulerian calculations were performed in parallel and an iterative self-consistent method was developed.

1 INTRODUCTION

Understanding the dynamics of multiphase systems is an issue of particular interest in the field of Computer Fluid Dynamics (CFD) applied to Nuclear Reactor Safety. A better knowledge of the forces that act on the bubbles moving in a continuous turbulent random fluid field is of importance for a complete description of the bubble's motion and to obtain for instance the radial and axial void fraction distribution inside the reactor channels.
Experiments specifically designed to understand the forces that act on the bubbles are a tool necessary to validate the models implemented inside the CFD codes. With this goal in mind, an upward isothermal co-current air-water flow in a vertical pipe (52 mm inner diameter) has been experimental investigated. Local measurements of void fraction, interfacial area concentration (IAC), interfacial velocity and Sauter mean diameter were measured using a four sensor conductivity probe. Liquid velocity and turbulence intensity were also measured using Laser Doppler Anemometry (LDA). Different air-water flow configurations were investigated for a liquid flow rate ranged from 0.491 m/s to 3 m/s and a void fraction up to 25 % .For each two-phase flow configuration twenty five radial position and three axial locations were measured by the conductivity probe methodology, and several radial profiles were also measured with LDA at different axial positions.
Numerical simulations of these experiments for bubbly flow conditions were performed by coupling a Lagrangian code that tracks the 3D motion of the individual bubbles in cylindrical

coordinates (r,ϕ,z) inside the fluid field under the action of the following forces: buoyancy, drag, lift, wall lubrication (Auton 1987, Antal at al.1991, Tomiyama et al 1997, 2002) Also we incorporate a 3D stochastic differential equation model to account for the random motion of the individual bubbles in the turbulent velocity field of the carrier liquid. This type of models denoted as continuous random walk models are used to predict the turbulent diffusion of the bubbles in the fluctuating velocity field of the carrier fluid (Bocksell and Loth 2006, Dehbi 2008). Also we have considered the deformation that suffers the bubbles when they touch the walls of the pipe and are compressed until they rebound.
The velocity and turbulence fields of the liquid phase were computed by solving the time dependent mass, energy, and momentum conservation equations in its Reynols Averaged Transport Equation form (RANS). The turbulent kinetic energy k, and the dissipation rate ε transport equations were simultaneously solved by using the k, epsilon model or the renormalized group model (RNG) model in a (r,z) grid by the finite volume method using the SIMPLER algorithm. Both Lagrangian and Eulerian calculations were performed in parallel because when integrating the 3D stochastic differential equations that take into account the motion of the bubbles in the fluid field we must consider the effect of the turbulence on the bubble's motion. To do this we must know the turbulence field that feels the bubble at each position along the path trajectory. Good predictions were obtained for the bubbles trajectories and the void fraction distribution in the channels when we consider that the lift radial force depends on the bubble's size and the bubbles are distorted, expressing this deformation in terms of the Eötvos number (Tomiyama 2002).

2 THE LAGRANGIAN MODEL FOR TRACKING THE BUBBLES

2.1 The forces acting on a single bubble

The bubble motion in cylindrical coordinates (r,θ,z) in the fluid field is governed by the following set of equations:

$$\left(\rho_g + C_v\rho_l\right)V_b\frac{d\vec{u}_b}{dt} = \sum_i \vec{F}_i \tag{2.1}$$

Where C_v is the coefficient of the virtual mass force which is assumed equal to 0.5, V_b is the volume of the bubble, and $\vec{F}_i$ are the different forces acting on the bubble. In cylindrical coordinates this equation is equivalent to the following set of equations:

$$\left(\rho_g + C_v\rho_l\right)V_b\left(\ddot{r} - r\dot{\theta}^2\right)_b = \sum_i F_{i,r} \tag{2.2}$$

$$\left(\rho_g + C_v\rho_l\right)V_b\left(r\ddot{\theta} + 2\dot{r}\dot{\theta}\right)_b = \sum_i F_{i,\theta} \tag{2.3}$$

$$\left(\rho_g + C_v\rho_l\right)V_b\,\ddot{z}_b = \sum_i F_{i,z} \tag{2.4}$$

Where $F_{i,r}, F_{i,\theta}, F_{i,z}$ are the radial, azimuthal and axial components of the i-th force acting on the bubble, and the point on the coordinate components means derivation with respect the time. The components of the velocity in cylindrical coordinates are denoted by $\left(u_r, u_\theta, u_z\right) = (\dot{r}, r\dot{\theta}, \dot{z})$.
The main forces that act on the bubble are the buoyancy force, the drag force, the lift force, the wall-lubrication force and the deformation force.
The buoyancy force acting on the bubble is directed in the positive axial direction and its components are given by:

$$F_{br} = 0,\ F_{b\theta} = 0,\ F_{bz} = V_b\left(\rho_l - \rho_g\right)g \tag{2.5}$$

The Drag force $\vec{F}_{Drag}$ acting on the bubble depends on the relative velocity between the bubble and the continuous phase (liquid), its components are given by the following expression:

$$\vec{F} = -\frac{3}{8}C_D\,\frac{1}{R_b}\,\rho_l\,V_b\,|\vec{u}_{rel}|\,\vec{u}_{rel} \tag{2.6}$$

Where $\vec{u}_{rel} = \vec{u}_b - \vec{u}_l$ is the relative velocity that feels the bubble at a given position in the liquid velocity field. For the Drag coefficient C_D we have used the expression given by Tomiyama (1997):

$$C_D = \beta\ \max\left[\min\left\{\frac{16}{\mathrm{Re}_b}\left(1+0.15\mathrm{Re}_b^{0.687}\right), \frac{48}{\mathrm{Re}_b}\right\}, \frac{8}{3}\frac{Eo_b}{Eo_b+4}\right] \tag{2.7}$$

Where Re_b and Eo_b are the Reynolds and the Eötvos numbers respectively for the bubble given by:

$$\mathrm{Re}_b = \frac{\rho_l|\vec{u}_b - \vec{u}_l|d_b}{\mu_l}, \quad Eo_b = \frac{g\ (\rho_l - \rho_g)\,d_b^2}{\sigma} \tag{2.8}$$

Finally, β is a experimental coefficient that is taken equal to one.

The experiments performed in vertical pipes with bubbly flow showed that relatively small bubbles tend to migrate toward the wall while large bubbles tend to migrate toward the centre. This lateral motion was attributed to the so called lift force, which it is due to the motion of a particle in a fluid with a velocity gradient in the movement direction; this gradient causes a shear field. The first analytical expression for the lift force was deduced by Auton (1987) for the case of a spherical particle moving in a velocity gradient of an inviscid fluid. Then this expression was extended by Tomiyama et al. that considered the interaction between the bubble and the shear field of the fluid (2002), and also considered the deformation of the bubble. This lift force acting on the bubbles is given according to Tomiyama (2002) by the following expression:

$$\vec{F}_{LF} = -C_T\,V_b\,\rho_l\left(\vec{u}_b - \vec{u}_l\right)\times\vec{\omega} \tag{2.9}$$

Where $\vec{\omega}$ is the vorticity of the continuous phase velocity field, $\vec{\omega} = \vec{\nabla}\times\vec{u}_l$ and C_T is the Tomiyama lift force coefficient that takes into account the interaction between the distorted bubble and the shear field and is given by:

$$C_T = \begin{cases} \min\left[0.288\tanh\left(0.121\mathrm{Re}_b\right), f\left(Eo_d\right)\right], & for\ Eo_d < 4 \\ f\left(Eo_d\right) & , for\ 4 < Eo_d < 10 \\ -0.27 & , for\ Eo_d < 10 \end{cases} \tag{2.10}$$

Where Eo_d is an Eötvos modified number, given in terms of the maximum horizontal dimension of the bubble d_{hb}

$$Eo_d = \frac{g\,(\rho_l - \rho_g)\,d_{hb}^2}{\sigma} \qquad \text{with } d_{hb} = d_b \sqrt[3]{1 + 0.163\,Eo^{0.757}} \tag{2.11}$$

And the function $f(Eo_d)$ is the same function defined by Tomiyama:

$$f(Eo_d) = 0.00105 Eo_d^3 - 0.0159\,Eo_d^2 - 0.0204\,Eo_d + 0.474 \tag{2.12}$$

We note that the coefficient C_T defined by Tomiyama becomes negative when the bubble diameter becomes bigger than 5.8 mm. This means that for big bubbles the lift force has opposite direction than for small bubbles.
The vorticity in cylindrical coordinates is computed by means of the expression:

$$\vec{\omega} = curl(\vec{u}_l) = \frac{1}{r}\begin{vmatrix} \hat{e}_r & r\hat{e}_\theta & \hat{e}_z \\ \frac{\partial}{\partial r} & \frac{\partial}{\partial \varphi} & \frac{\partial}{\partial z} \\ 0 & 0 & u_{lz}(r) \end{vmatrix} = -\frac{\partial u_{fz}(r)}{\partial r}\hat{e}_\theta \tag{2.13}$$

Because the CFD calculations shows that the velocity profile is logarithmic, we have assumed that the average fluid velocity profile in the z direction that is being used to compute the vorticity depends on the radial coordinate in the developed flow region and is given by:

$$\begin{aligned} u_{lz}(r) &= \left\{ \frac{1}{\kappa} \ln\left(\frac{(R-r)u^*}{\nu} \right) + B \right\} u^* \text{ , for } \quad 0 < r < R - \frac{5\nu}{u^*} \\ u_{lz}(r) &= \left\{ \frac{(R-r)u^*}{\nu} \right\} u^* \text{ , } \qquad\qquad \text{, for } \quad R - \frac{5\nu}{u^*} < r < R \end{aligned} \tag{2.14}$$

Where $u^* = \sqrt{\tau_w / \rho_l}$, being τ_w the shear stress at the pipe wall, and the constants B and κ are: B=5, and $\kappa = 0.41$ is the Von-Karman constant, and R is the pipe radius.
Therefore on account of equations (2.9), (2.13) and (2.14) the expression for the lift force is given in cylindrical coordinates by:

$$\vec{F}_{LF} = -C_T V_b\, \rho_f \left\{ (u_{bz} - u_{lz})\omega_\theta \hat{e}_r - (u_{br} - u_{lr})\omega_\theta \hat{e}_z \right\} \approx -C_T V_b\, \rho_f (u_{bz} - u_{lz})\omega_\theta \hat{e}_r \tag{2.15}$$

On account of equation (2.13) for the vorticity and equations (2.14) and (2.15), the lift force can be computed by means of the following expression:

$$\vec{F}_{LF} = \begin{cases} C_T V_b\, \rho_l (u_{bz} - u_{lz}) \left[\dfrac{u^*}{\kappa(R-r)} \right] \hat{e}_r \text{, for } 0 < r < R - \dfrac{5\nu}{u^*} \\ \\ C_T V_b\, \rho_l (u_{bz} - u_{lz}) \left[\dfrac{(u^*)^2}{\nu} \right] \hat{e}_r \text{ , for } R - \dfrac{5\nu}{u^*} < r < R \end{cases} \tag{2.16}$$

The next force considered in the model is the bubble deformation force. According to Zaruba et al (2007), we need to take on account this force to prevent the bubble centre of mass displacement to be unrealistically close to the wall. To compute this force we have assumed a

bubble that when approaching and touching the walls deforms and adopts an oblate shape as displayed at figure 1. We have assumed that the deformation of the bubble conserves the volume so we may write

$$\frac{4}{3}\pi R_b^3 = \frac{4}{3}\pi a^2 y \Rightarrow a = \frac{R_b^{3/2}}{y^{1/2}} \tag{2.17}$$

Where y is the distance from the wall to the bubble centre, and a denotes the dimension of the ellipsoid in the direction parallel to the wall. This ellipsoid is obviously oblate with $y < a$. The area of this ellipsoid can be calculated as the surface of a revolution spheroid with symmetry axis orthogonal to the wall. After some calculus this area is given by the expression:

$$S(y) = 2\pi a^2 + 2\pi a\, y \frac{\sinh^{-1}\mu'}{\mu'},\ with\ \mu' = \left(\frac{a^2}{y^2} - 1\right)^{1/2} = \left(\frac{R_b^3}{y^3} - 1\right)^{1/2} \tag{2.18}$$

The work that is needed to deform the bubble from the spherical form to the oblate one with distance y from the wall to the bubble centre is:

$$W(y) = \sigma \Delta S = \sigma\big(S(y) - S(y = R_b)\big) \tag{2.19}$$

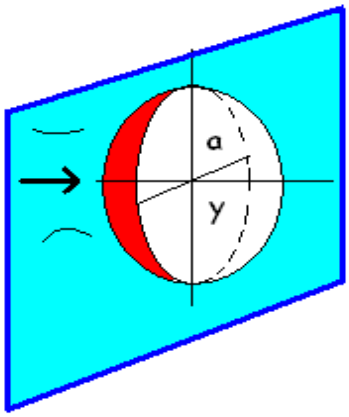

Figure 1 Bubble deforming while its gravity centre approach to the wall

Therefore the corresponding force acting on a single bubble with $y = R - r$ is given on account that $\hat{e}_y = -\hat{e}_r$ by:

$$\vec{F}_{Def} = -\frac{\partial W(y)}{\partial y}\hat{e}_y = 2\pi R_b \sigma \left(\frac{R_b}{y}\right)^{1/2} \left\{ -\left(\frac{R_b}{y}\right)^{3/2} + \frac{1}{2}\frac{\sinh^{-1}\mu'}{\mu'} + \frac{3}{2}\left(\frac{R_b}{y}\right)^3 \frac{1}{\mu'^{5/2}} \left(\sinh^{-1}\mu' - \frac{\mu'}{(1+\mu'^2)^{1/2}} \right) \right\} \hat{e}_r \tag{2.20}$$

This deformation force is directed toward the centre of the tube.

The last force considered in the Lagrangian model is the wall lubrication force. This force is originated as a consequence of the drainage of liquid around a bubble that is moving in the vicinity of the pipe wall. The non-slip condition at the wall should slow the drainage rate between the bubble and the wall, at the bubble-wall side, while the drainage of liquid is increased on the opposite side of the bubble. Therefore we have a asymmetrical drainage of liquid for a bubble moving close to the wall. As a consequence the bubble suffers a hydrodinamic force known as wall lubrication force. The expression for the force was first deduced by Antal et al (1991), and then improved by Tomiyama et al (1997):

$$\vec{F}_{WL} = -C_{WL}\, V_b\, \rho_l \left| u_{bz} - u_{lz} \right|^2 f_{wL}(r)\, \hat{e}_r \tag{2.21}$$

The coefficient of Tomiyama and Hosokawa (2002) for the wall lubrication force is given in terms of the bubble Reynolds number Re_b and the Eotvos bubble number, which is the ratio of the buoyancy to surface tension forces acting on the bubble:

$$C_{WL} = \max\left\{\frac{7}{\mathrm{Re}_b^{1.9}}, 0.0217\, Eo_b\right\} \tag{2.22}$$

And the function $f_{wL}(r)$, that defines the wall lubrication forces near the wall is:

$$f_{wL}(r) = d_b\left\{\frac{1}{(R-r)^2} - \frac{1}{(R+r)^2}\right\} \tag{2.23}$$

2.2 The model of turbulent diffusion by eddies and the connexion with the CFD model for the continuous phase.

For the numerical simulation of the continuous phase, the ideal method is to describe all the spatial and temporal scales down to the Kolmogorov scales, but this approach known as direct numerical simulation (DNS), is not practical for most of the engineering problems, since the numerical resources increase with the Reynolds number. A better approach commonly used to simplify the calculations is to predict the time-averaged velocity and the turbulence properties by solving the random averaged Navier-Stokes equations, and to use the turbulence parameters values k, ε obtained at the different points of the space $\vec{r}$ to build a statistical model that gives the instantaneous fluid fluctuation velocities that are seen by the bubbles in a Lagrangian frame.
Therefore, the average velocity of the fluid is computed by solving the random averaged Navier-Stokes equations (RANS) with the k, ε model in cylindrical coordinates. However the liquid velocity $\vec{u}_l = \vec{\bar{u}}_l + \vec{u}_l'$ that appears in equations (2.6), (2.9), (2.15), and (2.21) is composed of an average part $\vec{\bar{u}}_l$ that is computed solving the RANS equations and a fluctuating part $\vec{u}_l'$ due to the eddies that is obtained by a continuous random walk model in 3D, with isotropic turbulence, that in the region where the flow is completely developed we have assumed obeys the following Langevin equation (Bocksell and Loth 2006):

$$\frac{d\vec{u}_l'}{dt} = -\frac{\vec{u}_l'}{\tau_L(r,z)} + \left(\frac{2}{\tau_L(r,z)}\right)^{1/2}\sqrt{\frac{2k(r,z)}{3}}\,\vec{\xi}(t) \tag{2.24}$$

Where $k(r,z)$ denotes the turbulent kinetic energy per unit mass at point (r,z), and we have assumed to simplify the calculations that there is not azimuthal dependency by the symmetry of the problem, τ_L is the characteristic time of the Lagrangian time scale correlation (Dehbi 2008). Finally the vector $\vec{\xi}(\xi_r, \xi_\theta, \xi_z)$ denotes a Gaussian vector white noise random process, its components are independent Gaussian random numbers.
The model given by equation (2.24) assumes isotropic turbulence and no correlation between different components of the fluctuating fluid velocity. The characteristic time τ_L is computed away from the boundary layer by the following expression:

$$\tau_L(r,z) = 0.14\frac{k(r,z)}{\varepsilon(r,z)} \quad for \;\; y^+ = \frac{(R-r)u^*}{\nu_l} > 100 \tag{2.25}$$

At the boundary layer we have used the following expression computed by DNS by Kallio and Reeks (1989):

$$\tau_L^+(r,z)=10 \quad for \quad y^+=\frac{(R-r)u^*}{\nu_l}<5$$
$$\tau_L^+(r,z)=7.122+0.5731y^+-0.00129\left(y^+\right)^2 \;;5\le y^+=\frac{(R-r)u^*}{\nu_l}\le 100 \tag{2.26}$$

Where the non-dimensional Lagrangian time scale is defined by $\tau_L^+=\tau_L\frac{(u^*)^2}{\nu_l}$.

Equation (2.24) is equivalent to the following stochastic differential equation system:

$$d\vec{u}_l'=-\frac{\vec{u}_l'}{\tau_L(r,z)}dt+\left(\frac{2}{\tau_L(r,z)}\right)^{1/2}\sqrt{\frac{2k(r,z)}{3}}\,d\vec{W} \tag{2.27}$$

Where $d\vec{W}$ is a 3 dimensional Wiener process.
In computing the turbulence kinetic energy that appears in equations (2.24), (2.25) and (2.27) we must consider the turbulence induced by the bubbles in the liquid phase. We have considered that the turbulence kinetic energy induced by the bubbles depends on the void fraction and the Reynolds number for the bubbles so we write for the total turbulence to be considered in (2.27):

$$k=k_b+k_l \tag{2.28}$$

Where the turbulence k_b induced by the bubbles is given by the expression:

$$k=C_{lb}\,\alpha\,Re_b \tag{2.29}$$

Where the value of C_{lb} has been chosen equal to 5.5 10^{-5} , by comparison between the calculation results and the experimental data.

To finish this section we must say that when the bubbles move in the axial direction inside the pipe they expand its size because the pressure exerted by the liquid column diminishes. This expansion is computed by the program by taking into account the pressure of the water column over the bubble and the effect of the surface tension assuming that the gas inside the bubble behaves like a perfect gas.

3 GOVERNING EQUATIONS FOR THE CONTINUOUS CFD MODEL IN CYLINDRICAL GEOMETRY.

The time dependent Reynolds–Averaged governing equations for the momentum of the liquid continuous phase when no condensation is included and we assume that this phase behaves as a Newtonian incompressible fluid with stresses dominated by the turbulence is given by:

i) radial-component of the momentum equation

$$\alpha_l\rho_l\left(\frac{\partial\overline{u}_{l,r}}{\partial t}+\vec{\overline{u}}_l.\vec{\nabla}\overline{u}_{l,r}\right)=-\alpha_l\frac{\partial p}{\partial r}+\rho_l\left[\frac{1}{r}\frac{\partial}{\partial r}\left(-\alpha\,r\overline{u_{l,r}'^{\,2}}\right)+\frac{\partial}{\partial z}\left(-\alpha\overline{u_{l,r}'u_{l,z}'}\right)\right]+f_{i,r} \tag{3.1}$$

ii) z-component of the momentum equation

$$\alpha_l \rho_l \left(\frac{\partial \overline{u}_{l,z}}{\partial t} + \vec{\overline{u}}_l . \vec{\nabla} \overline{u}_z \right) = -\alpha_l \frac{\partial p}{\partial z} + \rho_l \left[\frac{1}{r} \frac{\partial}{\partial r} \left(-\alpha\, r \overline{u'_{l,r} u'_{l,z}} \right) + \frac{\partial}{\partial z} \left(-\alpha \overline{u'^{\,2}_{l,z}} \right) \right] - \alpha_l \rho_l g + f_{i,z} \tag{3.2}$$

Where $f_{i,r}, and\ f_{i,z}$ are the components of the interfacial forces per unit volume in the radial and axial directions respectively.

The Reynolds shear and normal stresses in the k-ε model are modelled by the effective viscosity formulation, which is a direct extension of the laminar deformation law:

$$\left(\tau_{r\,z}\right)_t = -\rho_l \ \overline{u'_{l,r} u'_{l,z}} = \mu_t \left(\frac{\partial \overline{u}_{l,r}}{\partial z} + \frac{\partial \overline{u}_{l,z}}{\partial r} \right) \tag{3.3}$$

$$\sigma_r = -\rho_l \overline{u'^{\,2}_{l,r}} = 2\mu_t \left(\frac{\partial \overline{u}_{l,r}}{\partial r} \right) - \frac{2}{3} \rho_l k \tag{3.4}$$

$$\sigma_z = -\rho_l \overline{u'^{\,2}_{l,z}} = 2\mu_t \left(\frac{\partial \overline{u}_{l,z}}{\partial z} \right) - \frac{2}{3} \rho_l k \tag{3.5}$$

Where the turbulent eddy viscosity is given according to Launder and Spalding (Launder and Spalding 1972) by:

$$\mu_{t,l} = c_\mu \ \rho_l \frac{k^2}{\varepsilon} \tag{3.6}$$

According to Dhotre, Smith and Niceno the incorporation of the bubble induced viscosity to μ_t did not alter the simulation results, so in this model we have not considered this contribution to the effective viscosity (Dhotre et al 2007), so the neglected contribution to the viscosity is :

$$\mu_{lb,l} = \rho_l \, C_{\mu lB} \, \alpha_g d_b \left| \overrightarrow{u_g} - \overrightarrow{u_l} \right| \tag{3.7}$$

We have used to calculate the turbulence energy and the dissipation rate the standard k, ε model with the model constants suggested by Launder and Spalding (Dhotre et al 2007).

4 EXPERIMENTAL FACILITY, INSTRUMENTATION AND EXPERIMENTS.

4.1 Description of the experiments

The experimental work was performed using a thermo-hydraulic loop placed at the Energy Engineering Institute in Polytechnic University of Valencia (Spain). The loop is schematically illustrated in Figure 2. It consists of a test section, a round transparent tube made by Plexiglas with constant section, an upper plenum and a lower plenum where air and water are mixed. The test section has a 52 mm inner diameter and a length of 3340 mm. The water was circulated by two centrifugal pumps controlled by a frequency controller.

The air was supplied by a compressor, and it was introduced to the test section through a porous sinter element with an average pore size of 10 mm installed below the mix chamber. The air and water temperature was kept constant during the test assay. The air mass flow rate was measured with a thermal mass flow meter and controller (Bronkhorst ® , EL-FLOW model), liquid flow rate with a Electromagnetic flow meter (Badger Meter ®), and the pressure with a precision pressure transmitter, DRUCK ® PTX 600 series.(INF position: range [0..1] bar, MED, SUP position range [0..250] mbar (Prec. 0.5% F.S.)

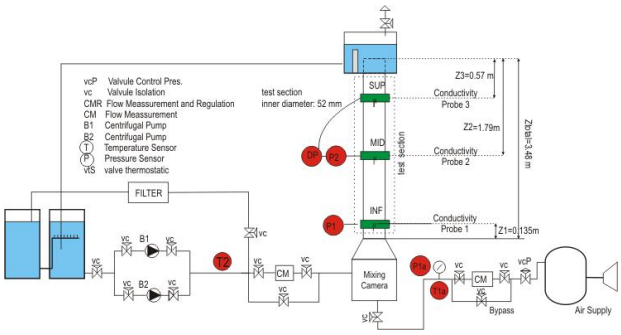

Figure 2: PUMA Facility scheme

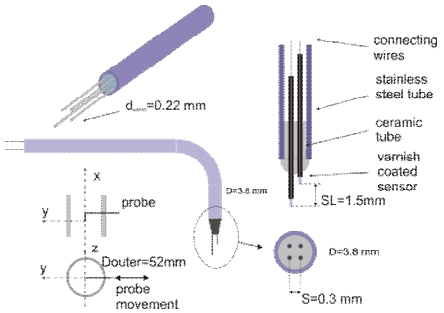

Figure 3: Schematic diagram of four sensor conductivity probe

The LDA (Laser Doppler Anemometry) equipment consists of a 0.5W Ar+ Ominichrome laser, Dantec Fiberflow beam separator, Dantec FVA 58N40 processor and a PC using the software Floware for data acquisition. A lens of 0.125 m focal length was used and the system was operated in backscattering mode. The vertical component was determined with green (λ=514.5 nm) beams and the horizontal component with blue (λ=488 nm) beams. A preshift frequency of 500 kHz was used. The flow was seeded with hollow particles which were neutrally buoyant with a 10 μm mean size (Dantec HGS-10); therefore, only the liquid velocity was measured. The time series obtained were 60 seconds long. The LDA system provides the liquid phase velocity moments. However, a number of data-processing steps are required before calculating the velocity moments. Firstly, the multiple validation, i.e. the multiple detection of the burst caused by a single particle, was handled by first rejecting velocity realizations with $u_{l,i} - \overline{u_{l,i}} > 4\sigma$ (σ is the standard deviation of the signal, $u_{l,i}$ denotes a single velocity realization and $\overline{u_{l,i}}$ denotes the averaged velocity over the measurement time). Then, the bursts which follow other bursts within a 1 ms interval were removed. Finally, the velocity bias, i.e. higher velocities over-representation, was corrected using the so-called 2D+ weighting: inversely weighting the data with the velocity. Since only two components are known, the magnitude of the third component is estimated from the variance of the second component so the weighting factor w is,

$$w = 1/\sqrt{u_{l,x}^2 + u_{l,z}^2 + \left(d_m / l_m\right)^2 \overline{u_{l,z}'^2}} \qquad (4.1)$$

with d_m/l_m as the diameter-to-length ratio of the ellipsoidal measurement volume. The use of only two components is justified since the magnitude of the vertical and lateral fluctuations will be close, and the influence of the third component is slight since d_m/l_m is also small. In this way, pairs of vertical and lateral velocity realizations, which have arrival times inside coincidence windows with a length of 200 μs, are searched. More technical details about the data processing can be found elsewhere (Harteveld et al. 2003, 2004).

4.2 Sensor conductivity probe methodology

The four- sensor probe is basically a phase identifier. It consists of two sensors made of stainless steel, coated with gold, with a diameter of 0.22 mm. The vertical distance between both tips was about 1.5 mm. Each sensor is insulated using an insulating varnish except its tips. If the probe is connected to a power supply with a fixed voltage, due to the large difference in conductivity between the liquid phase and the gas phase, the impedance signal acquired rises sharply when a bubble passes through one of the sensor tips, obtaining a more or less square signal. With a suitable signal processing methodology is possible to extract precise information from that raw signal.
From the time lag, between the impedance signals of the front and back tips, we can know the time that needs the front of the bubble to travel from one tip to the other that are far away a distance, S.

Then a measurable value of the bubble velocity, $u_{g,m}$, can be easily obtained. If the bubble moves with its velocity vector parallel to the conductivity probe orientation then the measurable value $u_{g,m}$ of the velocity match the true value of the bubble speed. However, as the bubble velocity fluctuates in response to the turbulence of the liquid phase then the bubble's lateral motion along with the finite value of the distance between both tips of the probe, and the bubble curvature can cause problems in the measurement of the true value of the bubble velocity. To quantify this difference it is possible to define a calibration factor as the ratio between the mean value and the measured value of the bubble including the missing bubbles. Calculations performed using the Monte-Carlo method show that for the range of velocities of the experiments performed at the PUMA facility the calibration factor is close to unity (Muñoz-Cobo et al 2007).

4.3 Set of experiments performed

Several sets of experiments were performed in PUMA facility with different j_g and j_l values. The goals and the characteristics of these experiments are displayed in table 1.

Table 1 Experiments performed at the PUMA facility of the UPV Institute for Energy Engineering

Experiments	Goal of the Experiments	Characteristics
F Number of runs 70	1-To measure the main local parameters of the two phase flow at 3 axial locations and 15 radial positions for each particular run 2-To measure the turbulence intensity and the liquid velocity at 2 axial position 3- To study the effect of the geometry of the conductivity probe of the measurements $j_f = 0.51, 1.023, 2.036, 3.086, 4.074$ $j_g = 0, 0.035, 0.077, 0.125, 0.176, 0.257, 0.338$ Two types of conductivity probes F0X, F0XA	5 different values of the liquid superficial velocity j_f, and 7 different values of the gas superficial velocity j_g. 2 different conductivity probe geometries. $5 \times 7 \times 2 = 70\ Runs$
A Number of runs 55	1-To study the transition from the bubbly flow regime to the slug flow 2-To study the evolution of the void fraction peak at the wall $j_f = 0.499 m/s$ $j_g = 0.0, 0.013, 0.035, 0.054, 0.097, 0.122, 0.142,$ $0.166, 0.188, 0.218, 0.237, 0.257, 0.305, 0.367$ $j_l = 1.006 m/s$ $j_g = 0.00, 0.029, 0.050, 0.081, 0.115, 0.150, 0.435, 0.528,$ $0.627, 0.736, 0.802, 0.173, 0.206, 0.257$ $j_l = 2.036 m/s$ $j_g = 0.0, 0.048, 0.093, 0.155, 0.224, 0.296, 0.35, 0.382,$ $0.477, 0.594, 0.740, 0.964, 1.357, 1.833$ $j_l = 2.956 m/s$ $j_g = 0.00, 0.026, 0.153, 0.289, 0.440, 0.606, 0.804,$ $1.02, 1.286, 1.618, 1.688$	4 different values of the liquid superficial velocity j_f and different values (14, 16,14,11) of the gas superficial velocity j_g $14 + 16 + 14 + 11 = 55$
B, C, D, E	1- To measure the effect of changes in the surface tension on the local parameters of the two phase flow.	Different properties of the liquid phase for

Number of Runs 80	2- To study the response of the conductivity probe to changes in the bubble size. The concentrations of 1-Butanol for the sets B,C,D, E are:0, 9, 39, 75 ppm	the same conditions of flow

The model results were compared with some of the experiments of the B-series when no butanol was added. The measurements with the conductivity probe were performed at 15 radial positions ranging from $r/R = 0.02$ to $r/R = 1$ and in three axial locations at $z/D = 2,36,56$, the geometry of the conductivity probe used for these experiments was the $F0XA$ and the LDA system was located only in one position at $z/D = 50$.

5 COMPUTATIONAL RESULTS AND COMPARISON WITH SOME EXPERIMENTS OF THE B SERIES

The dispersed phase is computed by tracking the bubbles along its trajectories. The bubbles are generated with a uniform distribution at the bottom of the pipe, and the diameter of the bubbles is sampled uniformly in the interval $[2.1mm, 2.9mm]$ according to the experimental data for the Sauter Mean Diameter. Then each individual bubble is tracked until it reaches a z coordinate of 3m, at this position the radial coordinate of each individual bubble and its volume is stored to compute the void fraction distribution. A total number of 8000 bubbles were tracked to obtain the void fraction distribution for each case. When each bubble moves in 3D along its trajectory its position changes and as a consequence the fluid velocity field that is being seen by the bubble also changes.

Because the turbulence field that is felt by the bubble has two components, one is the turbulence generated by the liquid and the other one is the turbulence induced by the bubbles. Because the fluctuating component of the liquid velocity field that is seen by the bubbles depends on the total turbulent energy $k(r,z)$ at each position (r,z), and to compute the turbulence induced by the bubbles we need the void fraction distribution, then we have performed several iterations to obtain a good void fraction distribution that is not known a priori. These iterations are performed as follow we start with the liquid turbulence alone in the continuous random walk model (CRW), then solving the RANS equations for the continuous phase and the Lagrangian model for the bubbles we obtain a first iterated value for the void fraction distribution that is more peaked than the experimental one because it does not take into account the random walk diffusion induced by the bubbles themselves. This distribution is used as an input to integrate the Lagrangian equations again and in this way we obtain a second iterated value of the void fraction distribution. After three or four iterations the void fraction distribution converges and gives values that are close to the experimental ones as displayed in figures 4 and 5.

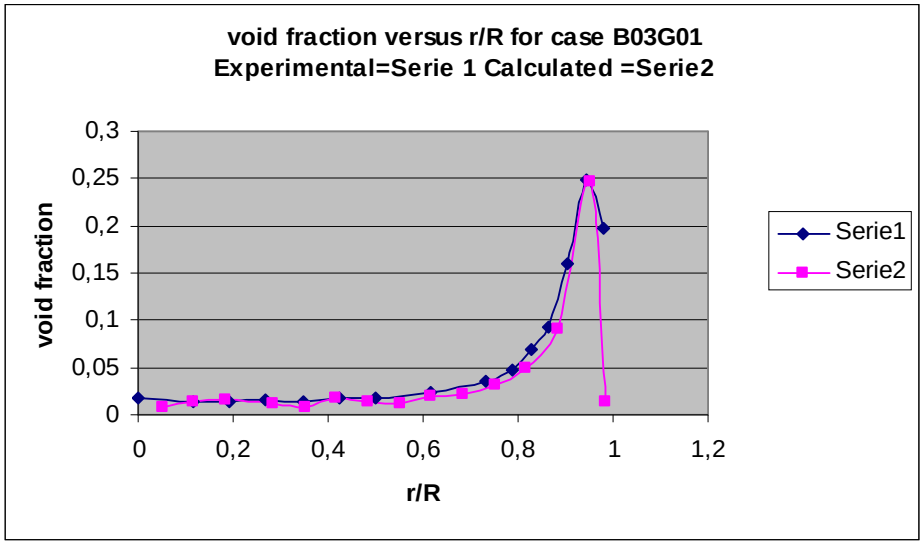

Figure 4 Void fraction versus r/R for case B03G01 Bubbly flow conditions with j_f=1.994m/s and j_g=0.134 m/s, with average void fraction $\overline{\alpha} = 0.0527$

The predictions of the void fraction distribution is very good in all the points, also the maximum position of the void fraction distribution and its value, it is well predicted by the Eulerian-Lagrangian model developed in this paper. The point near the wall has been computed a little bit near the wall than the experimental value. However it seems that the experimental value is higher than the computed one. This difference is due to the bubbles with diameters smallest than 2.1 mm. that slides over the liquid film close to the wall and that are not considered in the simulation.

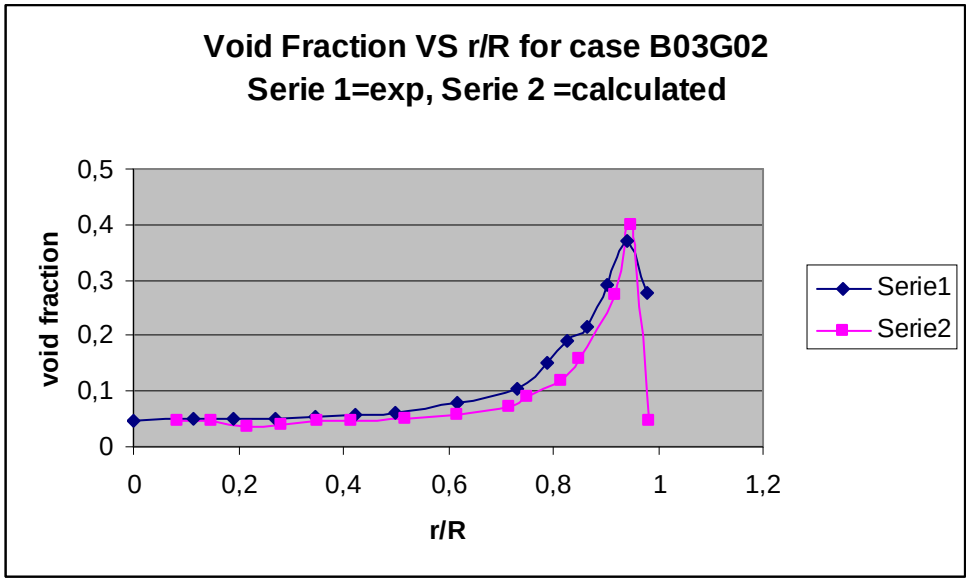

Figure 4 Void fraction versus r/R for case B03G02 Bubbly flow conditions with j_f=1.994m/s and j_g=0.347 m/s, with average void fraction $\overline{\alpha} = 0.0820$

6 CONCLUSIONS AND FUTURE DEVELOPMENTS

The Eulerian-Lagrangian model developped in this paper gives good prediction of the void fraction distribution for bubbly flow cases. The turbulence induced by the bubbles plays an important role in the Continuous Random Walk model because when this mechanism for turbulence production is not included, then the peak of the void fraction is higher than the experimental one. Because the void fraction distribution is not known a priori then a self-consistent calculation is performed in order to obtain the void fraction distribution. This is achieved by executing a set of iterations to obtain the true void fraction profile, the first void fraction distribution is obtained considering only the liquid turbulence. The output of this calculation is a first iterated void fraction distribution that is used as input for the second calculation and so on. The convergence is achieved in three or four iterations.

However this model does not included the coalescence of the bubbles, or the break up of the bubbles by interactions with turbulent eddies. So the next step is to include in this Eulerian-Lagrangian model the Break-Up and Coalescence mechanisms in order to go to the cap/slug regime, in this way we could make predictions of the void fraction distribution for several group of bubbles. The model is being improved by including these interaction mechanisms in a full Lagrangian-Eulerian model were group of bubbles are simultaneously tracked, when the distance between two bubbles is smaller than a certain distance an interaction take place.

Acknowlegdments

The authors of this paper are indebted to the National Plant of I+D by the support of the coordinated projects EXPERTISER ENE2007-68085-C02-01/CON and EXPERTISER ENE2007-68085-C02-02/CON to perform the experiments.

7 REFERENCES

Antal, S.P., Lahey Jr, R.T. and Flaherty, J.E."*Analysis of Two Phase Flow Distribution in Fully Developped Laminar Bubbly Two-Phase Flow*", Int. J.Multiphase Flow Vol17 ,635-652 (1991)

Auton, T.R., "The Lift Force on a Spherical Body in a Rotational Flow", Journal of Fluid Mechanics, vol183, pp 199-218 (1987)

Bocksell, T.L., Loth, E., "*Stochastic modelling of particle diffusion in a turbulent boundary layer*", Int. J. Multiphase Flow Vol 32, pp 1234-1253 (2006)

Dehbi, A., " *Turbulent particle dispersion in arbitrary wall-bounded geometries: a coupled CFD-Langevin-equation based approach*", Int. J.Multiphase Flow, Vol 34, pp 819-828 (2008)

Dhotre, M.T., Smith, B.L., Niceno, B." *CFD simulation of bubbly flows: Random dispersion model*". Chemical Engineering Science 62, pp 7140-7150 (2007)

Harteveld, W. K., Mudde, R. F. and Van den Akker, H. 2003. *"Dynamics of a bubble column: influence of gas distributions on coherent structures"*. Can. J. Chem. Eng. 81, 389-394.

Harteveld, W. K., Juliá, J. E., Mudde, R. F. and Van den Akker, H. 2004. *"Large scale vertical structures in bubble columns for gas fractions in the range of 5%-25%"*. CHISA Conference.

Hokosawa, S., Tomiyama, A., Misaki, S., Hamada, T. 2002 *"Lateral migration of single bubbles due to the presence of wall"*, Proceeding of ASME, Fluid Engineering Division, summer Meeting, Montreal.

Kallio, G.A., and Reeks, M.W., "*A numerical simulation of particle deposition in turbulent boundary layers*". Int. J. Multiphase Flow, 3, pp 433-446 (1989).

Muñoz-Cobo J.L., J. Peña, S. Chiva, S. Mendez, , 2006 *Monte-Carlo calculation of the calibration factors for the interfacial area concentration and the velocity of the bubbles for double sensor conductivity probe,* Nuclear Engineering and Design, Volume 237, Issue 5, March 2007, Pages 484-496.

Launder, B.E., Spalding, B., "Mathematical Models of Turbulence" Academic Press, New York (1972)

Tomiyama, A., Zun, I., Higaki, H., Makino, Y., Sakaguchi, T. "*A three dimensional particle tracking method for bubbly flow simulation"*. Nuclear Eng. and Design 175, pp 77-86 (1997).

Tomiyama, A., Tamai, H., Zun, I., Hosokawa, S. "*Tranverse migration of single bubbles in simple shear flows"* Chemical Engineering Science 57, pp 1849-1858 (2002).

Zaruba, A., Lucas, D., Prasser, H-M., Höhne, T., *"Bubble-wall interaction in a vertical gas-liquid flow: Bouncing, sliding and bubble deformations"*. Chemical Engineering Science Volume 62, pp 1591-1605(2007)..